Cake resistance of aggregates formed in the diffusion-limited-cluster-aggregation (DLCA) regime

Albert S. Kim [a,*], Rong Yuan [b]

[a] *Department of Civil and Environmental Engineering, University of Hawaii at Manoa, 2540 Dole Street, Honolulu, HI 96822, USA*
[b] *College of Mathematics, Qingdao University, Qingdao, Shandong 266071, PR China*

Abstract

The ideal aggregate characterized by the quadratically increasing permeability $\kappa(r) = k_2 r^2$ is investigated to estimate the specific cake resistance (i.e., inverse permeability) of a cake layer composed of deposited aggregates formed in the diffusion-limited-cluster-aggregation (DLCA) regime. Happel's cell model is employed in this study by embedding the ideal aggregate in the center of a spherical cell of tangential stress-free surface. The specific resistance is analytically calculated as a function of the occupancy fraction and then compared to those of conventional cake layers of equal-sized spherical colloids and uniformly porous spheres. The DLCA cake layer provides significantly less specific resistance and therefore shows the remarkable potential of aggregate-enhanced membrane filtration (AEMF) as a new protocol for colloidal filtration. The settling velocity of a swarm of the ideal aggregates is investigated as a by-product and experimental verification of this theory.
© 2006 Elsevier B.V. All rights reserved.

Keywords: Fractal aggregate; Cell model; Quadratic permeability; Cake resistance; Settling velocity; Aggregate-enhanced membrane filtration (AEMF)

1. Introduction

Conventional colloidal fouling in microfiltration (MF) and ultrafiltration (MF) can be classified into two categories, i.e., concentration polarization (CP) [1–6] and cake formation [5,7–11]. Particle morphology is effectively controlled by interparticle interactions (typically described by the Derjaguin–Landau–Verwey–Overbeek (DLVO) theory) [12,13] and hydrodynamic flow conditions [5,14]. Increasing ionic strength effectively suppresses the electrostatic double-layer repulsion [9,15,16] and causes a phase transition from liquid-like CP to solid-like cake [17]. At a high ionic strength and above the critical coagulation concentration (CCC) of the particle feed suspension, rapid aggregation can occur due to the dominant van der Waals forces [18,19]. Therefore, the diffusion-limited aggregation (DLA) and diffusion-limited cluster aggregation (DLCA) [20–22] occur with attractive primary particles and proceed faster than the reaction-limited aggregation [23–27].

Several experimental studies showed that pre-aggregation – defined in this study as aggregation of particles in the feed tank before the particles are introduced to the membrane surface – remarkably enhances the permeate flux of colloidal membrane filtration [28–31]. The deposited aggregates can be simply pictured as large porous particles of approximately the same size [32,33] (possibly) with varying permeability in the radial direction [34–36]. The sizes of porous aggregates are typically one or two orders of magnitude greater than the constituent primary particles [21,37,38] and therefore result in remarkable gains in the permeate flux [28–31]. This phenomenon is termed aggregate-enhanced membrane filtration (AEMF).

To predict performance of the AEMF protocol, quantification of the aggregate cake resistance is of crucial importance. The specific resistance, i.e., the cake resistance divided by the cake thickness is, in general, a function of average sizes, overall porosity, and fractal dimension of aggregates and primary particle size. One possible method is use of traditional permeability expressions [32,39–41], which is equivalent to replacing a highly porous aggregate by a volume-equivalent solid sphere of much smaller size. Another method is to generate a uniformly porous sphere of the same size as the fractal aggregate. Although the two methods provide a concep-

* Corresponding author. Tel.: +1 808 956 3718; fax: +1 808 956 5014.
E-mail address: Albert.S.Kim@hawaii.edu, AlbertSK@hawaii.edu
(A.S. Kim).
URL: http://www.pam.eng.hawaii.edu.

tual understanding in terms of equivalent spherical objects, in principle they cannot fully address effects of fractal structure on the hydrodynamic drag because aggregates have dense cores and sparse edges, providing a unique internal flow field [37,42].

It is worthwhile to review the historical development of hydrodynamic force estimation of spherical objects. Drag forces exerted on isolated spherical objects such as a solid sphere, a uniformly porous sphere, and a composite sphere (i.e., a solid sphere covered with a porous shell) were developed by Stokes, Brinkman [32], and Masliyah and Neale [43], respectively. Happel [40] developed a spherical cell model of free tangential stress to study hydrodynamic drag acting on a swarm of Stokes' solid spheres, and Neale et al. [44] replaced Stokes' solid sphere with Brinkman's uniformly porous sphere in Happel's cell model. This approach was extended by Kim and Yuan [45], who studied the creeping flow over a swarm of equal-sized composite spheres [43] and provided the most general solution of the five previous studies by Stokes [46,47], Brinkman [32], Masliyah and Neale [43], Happel [40], and Neale et al. [44]. Spherical objects in the above studies were solid, uniformly porous, or composite spheres, in which the aggregate fractality can be reflected only in approximate ways.

Several numerical studies were conducted to calculate the hydrodynamic drag force exerted on a (presumably) spherical aggregate characterized by its radius and fractal dimension [34,35,48]. They assumed either constant [48] or varying permeability [34,35] with Happel's model to link radial volume fraction and azimuthally uniform permeability. Aggregates of fractal dimensions less than two, such as formed in the DLCA regime [21], show tree-like branched structures. Therefore, Davies' experimental correlation for fibrous media [49] provided a better approximation rather than Happel's model, especially for sparse DLCA aggregates. While all the other works above were numerical studies for fractal aggregates with varying permeability, Kim and Yuan [36] derived the stream function and hydrodynamic drag force for an ideal aggregate of quadratically increasing permeability in the radial direction. By using Davies' correlation, they found that the ideal aggregate of the quadratic permeability highly corresponds to DLCA aggregates [21].

To systematically study the AEMF, an analytical representation of the specific cake resistance of a swarm of deposited aggregates is of great necessity. In the current theoretical poverty regarding aggregate-cake resistance, this study therefore aims to incorporate Happel's cell model [40] with Kim and Yuan's work [36] to derive the hydrodynamic resistance of a swarm of aggregates that are formed in the DLCA regime and then deposited on the membrane surface. Verification of this theory is performed by comparing experimental and theoretical studies in literature for hydrodynamic radius and settling velocity of DLCA aggregates.

2. Theoretical

A system of deposited DLCA aggregates on the membrane surface is mimicked by an ideal aggregate of radius b, lo-
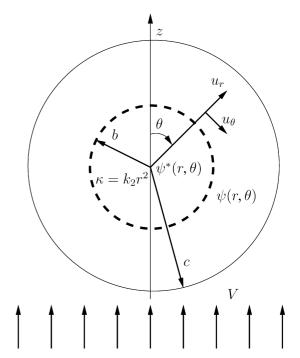

Fig. 1. Free-surface cell model applied to an isolated ideal aggregate with quadratically increasing permeability.

cated at the center of a spherical cell of radius c, as shown in Fig. 1. The ideal aggregate is illustrated as a porous sphere with quadratically increasing permeability in the radial direction [36]

$$\kappa(r) = k_2 r^2 \tag{1}$$

where k_2 is a permeability prefactor. Relative to the ideal aggregate, an azimuthal symmetry is applied to the creeping flow of Newtonian fluid with absolute viscosity in the steady state. Using this mathematical advantage, a spherical coordinate is selected as a reference frame, and only radial and tangential components are considered based on the axial symmetry. The incompressible Newtonian flow exterior to the aggregate is described by the Stokes and continuity equations and, inside the ideal aggregate, conservation of momentum is represented by the Brinkman and continuity equations. The effective viscosity within the aggregate is assumed to be equal to the absolute fluid viscosity. The boundary conditions incorporated in this study are (i) finite velocity field at the center of the aggregate, i.e., $r = 0$, (ii) continuity of flow field and stress tensor components at the aggregate surface, i.e., $r = b$, and (iii) the vanishing tangential stress at the surface undergoing the ambient fluid velocity V such as

$$\tau_{r\theta}(c, \theta) = 0 \tag{2}$$

$$u_r(c, \theta) = V \cos \theta \tag{3}$$

with $0 < \theta < 2\pi$, where $\tau_{r\theta}$ and u_r represent the tangential stress tensor and radial velocity component, respectively. Although employing a different type of boundary condition [50] is possible by considering vorticity instead of tangential stress, this study follows the historical development of Happel's cell

model [40,44,45] using Eq. (2) for theoretical consistency. Details of mathematical representations can be found in our previous work [36]. The continuity and azimuthal symmetry of the fluid flow give the mathematical simplicity under which stream functions outside and inside the aggregate are represented as [36]

$$\psi(\xi, \theta) = -\frac{1}{2} V b^2 (A\xi^{-1} + B\xi + C\xi^2 + D\xi^4) \sin^2 \theta \text{ for } \xi \geq 1$$

(4)

and

$$\psi^*(\xi, \theta) = -\frac{1}{2} V b^2 (E\xi^{n_1} + F\xi^{n_2} + G\xi^{n_3} + H\xi^{n_4}) \sin^2 \theta$$

for $\xi \leq 1$ (5)

respectively, where $\xi = r/b$, and

$$n_1 = \frac{3}{2} - \frac{1}{2}\sqrt{13 + \frac{2}{k_2} + 2\sqrt{36 - \frac{4}{k_2} + \frac{1}{k_2^2}}},$$

$$n_2 = \frac{3}{2} - \frac{1}{2}\sqrt{13 + \frac{2}{k_2} - 2\sqrt{36 - \frac{4}{k_2} + \frac{1}{k_2^2}}},$$

$$n_3 = \frac{3}{2} + \frac{1}{2}\sqrt{13 + \frac{2}{k_2} - 2\sqrt{36 - \frac{4}{k_2} + \frac{1}{k_2^2}}},$$

$$n_4 = \frac{3}{2} + \frac{1}{2}\sqrt{13 + \frac{2}{k_2} + 2\sqrt{36 - \frac{4}{k_2} + \frac{1}{k_2^2}}}$$

(6)

To satisfy the boundary conditions described above, the eight arbitrary constants in Eqs. (4) and (5), A to H, should have specific analytic forms:

$$A = \frac{[(n_3 - 1)(n_3 - 2)(n_4 - 1)(n_4 - 2)k_2 + n_3 n_4 - 2]\gamma^6}{J_\gamma}$$

(7)

$$B = \frac{1}{J_\gamma}\{3[-(n_3 + 1)(n_3 - 2)(n_4 + 1)(n_4 - 2)k_2 - 2 - n_3 n_4]\gamma^6$$

$$+ 2[-(n_4 - 2)(n_4 - 4)(n_3 - 2)(n_3 - 4)k_2 + 8 - n_3 n_4]\gamma\}$$

(8)

$$C = \frac{1}{J_\gamma}\{2[(n_3 - 1)(n_3 + 1)(n_4 - 1)(n_4 + 1)k_2 + n_3 n_4 + 1]\gamma^6$$

$$+ 3[(n_3 - 1)(n_3 - 4)(n_4 - 1)(n_4 - 4)k_2 + n_3 n_4 - 4]\gamma\}$$

(9)

$$D = \frac{[-(n_3 - 1)(n_3 - 2)(n_4 - 1)(n_4 - 2)k_2 - n_3 n_4 + 2]\gamma}{J_\gamma}$$

(10)

$$E = 0$$ (11)

$$F = 0$$ (12)

$$G = \frac{6}{J_\gamma(n_4 - n_3)}\{-[-(n_4 - 1)(n_4 - 2)(n_4 + 1)k_2 + n_4]\gamma^6$$

$$- [-(n_4 - 1)(n_4 - 2)(-n_4 + 4)k_2 - n_4]\gamma\}$$

(13)

$$H = \frac{6}{J_\gamma(n_4 - n_3)}\{-[(n_3 - 1)(n_3 - 2)(n_3 + 1)k_2 - n_3]\gamma^6$$

$$- [(n_3 - 1)(n_3 - 2)(-n_3 + 4)k_2 + n_3]\gamma\}$$

(14)

where

$$J_\gamma = \{2[(n_4 - 1)(n_4 + 1)(n_3 - 1)(n_3 + 1)k_2 + n_3 n_4 + 1]\gamma^6$$

$$+ 3[-(n_4 + 1)(n_4 - 2)(n_3 + 1)(n_3 - 2)k_2 - n_3 n_4 - 2]\gamma^5$$

$$+ 3[(n_4 - 1)(n_4 - 4)(n_3 - 1)(n_3 - 4)k_2 + n_3 n_4 - 4]\gamma$$

$$- 2(n_4 - 2)(n_4 - 4)(n_3 - 2)(n_3 - 4)k_2 - 2n_3 n_4 + 16\}$$

(15)

and

$$\gamma = \frac{c}{b} \geq 1$$ (16)

Integrating the net z-component of the normal and tangential stress distributions over the entire aggregate surface yields the hydrodynamic drag force acting on the ideal aggregate:

$$F_{\text{drag}} = 2\pi b^2 \int_0^\pi [\tau_{rr} \cos \theta - \tau_{r\theta} \sin \theta]_{r=b} \sin \theta \, d\theta$$

$$= 6\pi\mu V b \Omega_Q$$

(17)

where

$$\Omega_Q(k_2, \gamma) = -\frac{2}{3}B$$ (18)

The physical meaning of Ω_Q is the ratio of hydrodynamic drag force experienced by the ideal aggregate of radius b in the aggregate swarm to the force exerted on an isolated impermeable sphere of the same radius. The subscript Q stands for the quadratic permeability of the ideal aggregate. Here, the specific cake resistance r_c, defined as the cake resistance divided by the cake thickness (i.e., the linear resistance gradient) or the inverse permeability of the cake layer [45], can be expressed as:

$$r_c = \frac{\Omega_Q}{2b^2/9\lambda}$$ (19)

where $\lambda = 1/\gamma^3$, which is defined as the occupancy fraction [45] and always greater than the volume fraction ϕ of the aggregate cake because of the porous space within the ideal aggregate. It is worth noting that the denominator of Eq. (19) stands for the permeability of solid impermeable spheres of radius b in a dilute limit when λ is interpreted as the volume fraction of the spheres.

3. Results and discussion

3.1. Convergence to previous work

With a finite occupancy fraction of λ, Happel's correction factor can be retrieved by taking the limit of $k_2 \to 0$, i.e.

$$\lim_{k_2 \to 0} \Omega_Q \equiv \Omega_H = \frac{1 + (2/3)\lambda^{5/3}}{1 - (3/2)\lambda^{1/3} + (3/2)\lambda^{5/3} - \lambda^2} \quad (20)$$

In this case, the ideal aggregate becomes an impermeable solid sphere so that any flow cannot penetrate the interior of the ideal aggregate. The occupancy fraction $\lambda(= b^3/c^3)$ of the ideal aggregate is therefore transformed into the volume fraction of equal-sized spherical particles of the same radius b.

The single presence of the ideal aggregate is described by taking the limit of $\gamma \to \infty$ so that the outer cell of radius c of Fig. 1 disappears accordingly. Then, the eight coefficients, A to H, of Eqs. (7)–(14) become identical to those obtained in Kim and Yuan's previous work [36]. They used equality of the quadratic permeability in Eq. (1) to Davies' experimental correlation, approximated as

$$\kappa = \frac{a_p^2}{16\phi^{1.5}(1 + 56\phi^3)} \simeq \frac{a_p^2}{16}\phi^{-3/2} \quad (21)$$

with the fractal profile of the radial volume fraction

$$\phi = \frac{1}{3}k_f D_f \left(\frac{r}{a_p}\right)^{D_f - 3} \quad (22)$$

where a_p is the primary particle radius and D_f is the fractal dimension. The average volume fraction is calculated as

$$\langle \phi \rangle = \frac{1}{(4\pi/3)b^3} \int_0^b \phi(r)4\pi r^2 \, dr = k_f \left(\frac{b}{a_p}\right)^{D_f - 3} \quad (23)$$

So, the average aggregate porosity is

$$\langle \epsilon \rangle = 1 - k_f \left(\frac{b}{a_p}\right)^{D_f - 3} \quad (24)$$

After Eq. (22) is substituted into Eq. (21), the exponent of r is equated to two, as in Eq. (1). Then, the calculated fractal dimension is

$$D_f = 3 + 2 \times (-)\frac{2}{3} = \frac{5}{3} = 1.67 \quad (25)$$

which is slightly lower than the typical fractal dimension of 1.75 in DLCA aggregates [21]. The approximation used in Eq. (21) is more valid for porous structures of low volume fraction ϕ, such as sparse DLCA aggregates.

The relationship between the total number of primary particles, N, within the aggregate is

$$N = k_f \left(\frac{b}{a_p}\right)^{D_f} \quad (26)$$

where k_f is a proportionality constant, which is linked to k_2 as

$$k_2 = \frac{27}{16}(5k_f)^{-3/2} \quad (27)$$

Sorenson and Robert [51] used a similar relationship, i.e.

$$N = k_0 \left(\frac{R_g}{a_p}\right)^{D_f} \quad (28)$$

with the gyration radius of the aggregate given as [52]

$$R_g = b\sqrt{\frac{D_f}{D_f + 2}} \quad (29)$$

and performed DLCA simulations that created 24 different aggregates in three dimensional space to find a correlation between k_0 and D_f. From their results, we take $k_0 = 1.60$ for $D_f = 1.67$ and calculate the values of k_f and k_2 as 0.83 and 0.20, respectively.

3.2. Comparison to other work

Our approach can be verified in terms of settling velocities of fractal aggregates, investigated by theoretical, simulational, and experimental ways. In general, aggregates have irregular internal structures due to their fractal nature [53–55]. Because of technical difficulties in locating coordinates of constituent primary particles within aggregates, settling velocity of whole aggregates is often measured and used to correlate the number of primary particles, aggregate size, mass density, and fractal dimension using modified Stokes' law [56–58]. Although the overall porosity of an aggregate reflects the fractal dimension into the power law as shown by

$$1 - \epsilon \propto \left(\frac{b}{a_p}\right)^{D_f - 3} \quad (30)$$

the modified Stokes' law still treats a fractal aggregate as a uniformly porous sphere of porosity ϵ.

In this light, Li and Logan [59] developed the cluster-fractal model, in which an aggregate is considered to be a collection of a number of smaller aggregates, called fractal generator of the same fractal nature. This model is, therefore, suitable for investigating tenuous aggregates formed in a DLCA regime. Li and Logan [59] defined a dimensionless settling velocity, Γ, as

$$\Gamma = \frac{U_a}{U_s} \quad (31)$$

where U_a and U_s are the respective settling velocities of an aggregate and an impermeable sphere of the same mass with a common radius, b. The identical bulk mass density, ρ_b, for both the aggregate and impermeable sphere is

$$\rho_b = \rho_p(1 - \epsilon) + \rho_f \epsilon \quad (32)$$

where ρ_p and ρ_f are mass densities of the primary particle of radius a_p and the fluid, respectively. In this case, the settling velocity ratio, Γ, of an ideal aggregate can be also expressed using Ω_Q as

$$\Gamma = \frac{U_a}{U_s} = \frac{6\pi\mu b U_a/(F_g - F_b)}{6\pi\mu b U_s/(F_g - F_b)} = \frac{1}{\Omega_Q} \quad (33)$$

where F_g and F_b are gravitational and buoyant forces equally exerted in magnitude on the aggregate and impermeable sphere.

Li and Logan [59] calculated $\Gamma = 1.7$ with $D_f = 1.7$ using the cluster-fractal model for large aggregates composed of more than 30 fractal generators. They also verified the model by comparing it with a previous experimental study of the settling velocity ratio of $\Gamma = 2.3$ with $D_f = 1.81$, which provided good agreement of their theoretical and experimental results [60]. Similar experimental studies on the fractal dimension can be found elsewhere [56]. Our current model development is specifically for DLCA aggregates, of which fractal dimension is (about) 1.67. Using the designated fractal dimension, we calculated $\Omega_Q(k_2 = 0.2, \gamma \to \infty) = 0.59$ so $\Gamma = 1/0.59 = 1.69$, which provides excellent agreement with Li and Logan's theoretical work, which has been experimentally validated.

The current theory can be compared with Chen et al.'s work [61] in terms of the ratio of hydrodynamic radius, R_h, to gyration radius, R_g, of the ideal aggregate. They created 133 DLCA aggregates with different numbers of primary particles and indicated $R_h/R_g = 0.875$ regardless of the cluster sizes. Using $D_f = 1.67$ and $k_2 = 0.2$, we performed the same calculation of the R_h/R_g ratio as

$$\frac{R_h}{R_g} = \frac{b\Omega_Q}{b\sqrt{D_f/(D_f+2)}} = \Omega_Q\sqrt{\frac{D_f}{D_f+2}} \qquad (34)$$

and obtained a value of 0.875, which is identical to Chen et al.'s work [61]. Their fractal dimension of the DLCA aggregates is 1.78, which is very close to Weitz and Olivera's experimental observation [21] and slightly higher than 1.67.

For additional comparison, we also used our mapping method of a composite sphere (i.e., a solid spherical core covered with a porous shell) on an arbitrary aggregate [45]. For this analysis, the same values of D_f and k_2 are used for the number of constituent primary particles varying from 50 to 5000. Results are shown in Table 1 and indicate that R_h/R_g values are almost independent of the number of primary particles, N, having an average value of 0.8714 ± 0.0036. All values of the R_h/R_g ratio are between 0.868 and 0.878, a range in which Chen et al.'s result of 0.875 readily falls.

Furthermore, the settling velocity of a swarm of the ideal aggregates can be easily analyzed using the current model. The dimensionless settling velocity v_s is defined as [45]

$$v_s \equiv \frac{\Omega_Q^{-1}(\gamma)}{\Omega_Q^{-1}(\gamma \to \infty)} = \frac{\Omega_Q(\lambda \to 0)}{\Omega_Q(\lambda)} \qquad (35)$$

Table 1
Ratio of hydrodynamic radius to gyration radius calculated using the mapping method [45]

N	R_h/a_p	R_g/a_p	R_h/R_g
50	6.896	7.855	0.878
100	10.401	11.895	0.874
300	20.006	22.966	0.871
500	27.135	31.183	0.870
1000	41.053	47.226	0.869
3000	79.185	91.176	0.868
5000	107.496	123.801	0.868

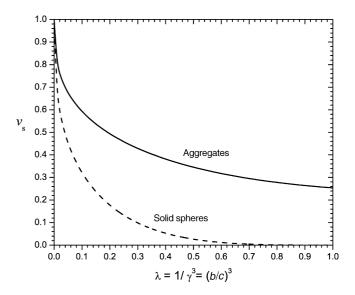The mean and standard deviation of R_h/R_g values are 0.8714 and 0.0035, respectively.

Fig. 2. Dimensionless settling velocity v_s of a swarm of the ideal aggregates and solid spheres as functions of λ, the occupancy fraction for aggregates and volume fraction of the solid spheres.

which is a ratio of the settling velocity of a swarm of the ideal aggregates to that of a single aggregate in an unbound fluid medium. Fig. 2 shows the plot of v_s versus λ and indicates that the settling velocity of the aggregate swarm is comparable to that of the isolated aggregate: $v_s(\lambda = 1)$ is only 25% of $v_s(\lambda = 0)$. The swarm of solid spheres settles faster than the aggregate swarm if the solid spheres have the same aggregate sizes as well as the same density of constituent primary particles. The dimensionless velocity of a swarm of solid impermeable sphere can be described by

$$v_s = \frac{1}{\Omega_H(\lambda)} \qquad (36)$$

which is compared with Eq. (35) in Fig. 2. As the volume fraction exceeds 0.4, the settling velocity of the solid-sphere swarm is negligible in comparison to that of a single impermeable sphere, indicating significant hindered settling behavior [62–64].

3.3. Specific cake resistance

Fig. 3 shows Ω's of Happel's, Neale et al.'s, and our models as functions of λ, commonly defined as b^3/c^3. In the current and Neale et al.'s study, λ is the occupancy fraction of a swarm of porous aggregates, but in Happel's cell model it is interpreted as the volume fraction of a collection of solid spheres. Presence of the solid sphere as well as the ideal aggregate, commonly having the radius of b, is revisited by taking the limit of $\lambda \to 0$, i.e., $c \to \infty$. The convergence of Happel's cell model to Stokes' law is represented by $\Omega_H(\lambda = 0) = 1$. The $\Omega_Q(\lambda = 0)$ value of 0.59 is a reproduction of Kim and Yuan's work [36] and indicates that an isolated ideal aggregate generates 59% of the resistance caused by solid spheres of the same radius in an infinitely dilute limit.

As λ increases to 1, Ω_H diverges to infinity, implying that the cake layer becomes impermeable so that no solvent can pass through the layer. However, mono-dispersed spheres can gener-

ate the highest volume fraction, as much as 0.74, with a perfect face-centered-cubic (fcc) structure [65–67]. Random packing of equal-sized spheres renders a volume fraction that ranges from 0.58 to 0.64 [68–72]. The value of Ω_H with $\lambda = 0.64$ is 123.21, indicating that the specific resistance of a cake layer composed of mono-dispersed spheres with a volume fraction of 0.64 is two orders of magnitude greater than that of a swarm of the same spheres in an infinitely dilute limit where Stokes' law is an excellent approximation. This reemphasizes that the conventional colloidal cake resistance from individual (unaggregated) particles is a major source of permeate flux decline in MF and UF processes.

A comparative analysis of Ω_Q and Ω_{NEN} in Fig. 3 was conducted as follows. $\Omega_{NEN}(\beta, \lambda)$ is a hydrodynamic correction factor for a swarm of equal-sized, uniformly porous spheres with β, defined as

$$\beta = \frac{b}{\sqrt{\kappa_0}} \qquad (37)$$

where κ_0 is the uniform permeability due to homogeneous mass distribution within the uniformly porous sphere. To compare the hydrodynamic drags exerted on a swarm of ideal aggregates and that of homogeneous spheres of the same size b, κ_0 is set as a volume-averaged value of the quadratically increasing permeability of Eq. (1), i.e.

$$\kappa_0 = \langle \kappa(r) \rangle = \frac{1}{(4\pi/3)b^3} \int_0^b k_2 r^2 4\pi r^2 \, \mathrm{d}r = \frac{3}{5} k_2 b^2 \qquad (38)$$

Substitution of Eq. (38) into (37) with $k_2 = 0.2$ yields

$$\beta = \sqrt{\frac{5}{3k_2}} = 2.887 \qquad (39)$$

Using this value of β, Ω_{NEN} is plotted with Ω_Q in Fig. 3. For all λ, i.e., from isolated ($\lambda = 0$) to fully packed ($\lambda = 1$) spherical objects, Ω_{NEN} is always less than Ω_Q (although it is not
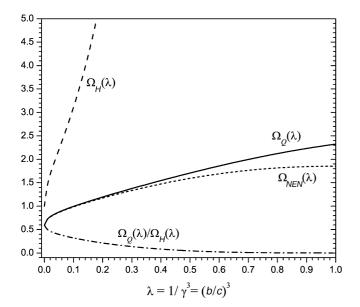

Fig. 3. Correction factors of Happel's (Ω_H), Neale et al.'s (Ω_{NEN}), and the current (Ω_Q) models.

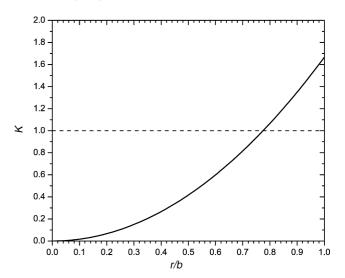

Fig. 4. Dimensionless radial permeability, $K = (5/3)(r/b)^2$ as a function of the dimensionless radial distance, r/b.

highly visible for small λ). Permeability-equivalent homogeneous spheres undergo less hydrodynamic drag than ideal aggregates with radially varying permeability. This phenomenon can be explained by investigation of the dimensionless radial permeability defined as

$$K = \frac{\kappa(r)}{\langle \kappa(r) \rangle} = \frac{5}{3} \left(\frac{r}{b} \right)^2 \qquad (40)$$

as shown in Fig. 4. The uniformly porous spheres have a constant permeability with respect to the radial position so that more flow can penetrate the central interior of the porous spheres, causing less drag, although their edge regions are less permeable than that of the ideal aggregates. The dimensionless permeability K is negligible where $r/b < 0.3$, and it becomes equal to the mean value at $r/b = \sqrt{3/5} = 0.775$. This indicates that a composite sphere model [45] could be a better alternative than a uniformly porous sphere as supported by the results noted in Table 1.

The limit of $\lambda = 1$ is physically impossible for a conventional colloidal cake, but it can be analyzed for the aggregate-cake layer. While deposited aggregates are partially overlapped, several of the longest branches of the aggregates that touch can be broken, and therefore detached monomers and/or groups of primary particles can be generated. The broken pieces can be reattached to their parent or other nearby aggregates. On the other hand, if edge-overlaps are present with minimum breakage of aggregate branches, $\lambda = 1$ implies that overlapped inter-spaces are equal to the inter-void-spaces between aggregates. It is obvious that high pressure can demolish the fractal structure of deposited aggregates and therefore cause cake collapse to a certain extent, depending on the mechanical strength of the fractal dimension of aggregates [73].

If packed spherical objects are porous, the formed cake layer provides much less hydrodynamic specific resistance, i.e., much more permeability, in comparison to that of solid objects. In other words, as the occupancy ratio λ approaches 1, Ω_Q reaches 2.32, which implies that a cake layer fully packed with the ideal DLCA aggregates provides a specific resistance of only as much as 2.32 times of the resistance caused by solid spheres (of the

same size) in an infinitely dilute limit (such as the CP phase). Further overlap and breakage of deposited aggregates may increase the value of $\Omega_Q(\lambda \to 1) = 2.32$. However, the curve of Ω_Q/Ω_H in Fig. 3 indicates that for $\lambda \geq 0.3$ the specific resistance of the DLCA-aggregate cake is less than 10% of the conventional colloidal cake resistance of individual spherical particles. This reflects the remarkable potential of the AEMF as a new paradigm for colloidal filtration processes by noting that the specific resistance is solely proportional to the inverse squared radius of deposited spherical objects if volume fractions are kept constant regardless of the radius.

The uniqueness of Kim and Yuan's theory of the quadratic permeability is that effects of primary particle size a_p on the correction factor Ω_Q disappear entirely so that the specific cake resistance solely depends on the radius b of the aggregate with the specific fractal dimension, 1.67. As the fractal profile of the radial volume fraction generally indicates, a larger ideal aggregate has a sparser structure near its edge (i.e., $r = b$). The full connectivity of constituent primary particles preclude continuous growth of the aggregates (in the feed tank), keeping their fractal nature. Given that the environment for aggregation is limited by diffusion of primary particles, overall size of the aggregates is dependent on the primary particle size (with given net attractive inter-particle interactions). Then, a ratio can be defined as

$$s = \frac{b}{a_p} \tag{41}$$

and Eq. (19) can be rewritten as

$$r_c = \frac{10.44}{a_p^2 s^2} \tag{42}$$

with $\lambda = 1$ and so $\Omega_Q = 2.32$. The typical value of 's' is of an order of a few tens, and for large aggregates it can reach and exceed (about) 10^2 [61]. With known a_p and measured s (averaged with a number of aggregates) using certain experimental techniques [31,74–76], one can estimate the specific cake resistance of aggregates, formed in the DLCA regime with a fractal dimension of about 1.7. Excess applied pressure and/or continuous build-up of the aggregates on the membrane surface induce further overlap and compression of deposited aggregates and may eventually cause cake collapse [73], in which case Eq. (42) may underestimate the specific resistance. A comparative study that analyzes geotechnical consolidation and cake formation can be found elsewhere [77]. Total collapse of the aggregate cake, due to lack of sufficient mechanical forces to sustain the structure, will compel revisiting theories on the conventional filtration of colloidal cake formation, which is beyond the limit of the current theory.

Waite et al.'s [31] and Hwang and Liu's [29] experimental observations are closely related to applications of the current theory. Waite et al. used 70 nm hematite primary particles and measured two different aggregation regimes, i.e., rapid and slow aggregation with fractal dimensions of 2.20 and 2.35, respectively. The rapid aggregation at high ionic strength provided a higher permeate flux than the slow aggregation with low ionic strength. The high ionic strength suppressed the electrostatic repulsion;

therefore, the primary particles were attractive or less repulsive due to the dominant van der Waals interactions. Although measuring fractal dimensions using the small angle light scattering technique is subjective to human eyes, most aggregates formed in both the rapid and slow aggregation regimes seemed to have physical properties of the reaction-limited aggregation, i.e., fractal dimensions generally greater than 2 [26,27,78,79]. Hwang and Liu's study also showed that as the ionic strength increases, aggregate size increases, providing higher permeate flux. Their aggregates have, however, average sizes that are only a few times greater than that of primary particles, and hence are too small to be treated as fractal objects but possibly as fractal-like structures due to the limited number of constituent primary particles [80]. To compare the above experimental results with our theory, we calculated the specific resistance of Eq. (42) and found that our theory gives at least several factors or one order of magnitude smaller specific resistance than their experimental observations. This deviation of the theoretical results from experimental data mainly stems from the fractal nature of the aggregates used in experiments, i.e., RLCA-like structure and/or small aggregate size.

To the best of our knowledge, sophisticated filtration experiments with DLCA aggregates of fractal dimensions about 1.7–1.8 have not been reported in the current literature. The current theory is, however, consistently analyzed by comparing other theoretical [59], simulational [61], and experimental [29,31,60] studies. The expression for the specific resistance of aggregate cake will be, therefore, a better approximation if the deposited aggregates keep their DLCA-fractality with less overlap and breakage, having a smaller size ratio, s, of an order of $O(10^1)$.

4. Concluding remarks

The drag force experienced by an aggregate with quadratically increasing permeability in a swarm of identical aggregates was derived using the Stokes, Brinkman, and continuity equations. A tangential stress-free cell model was employed to mimic the presence of the aggregate-swarm. The analytic solution was used to estimate the specific resistance of a cake layer composed of deposited DLCA aggregates characterized by a fractal dimension of about 1.7. The settling velocity of the swarm of the aggregates was also studied as a function of the occupancy fraction and experimentally verified. In comparison to the conventional colloidal cake consisting of individual spherical colloids, the aggregate cake layer provided significantly less resistance, implying that the pre-aggregation of particles – before they are introduced to the membrane surface – can remarkably increase the permeate flux of typical MF and UF processes. Our theoretical prediction for the aggregate cake layer is restricted to (small) DLCA aggregates, and strong inter-aggregate overlap possibly followed by entire cake collapse is beyond the limit of the current theory.

References

[1] S. Bhattacharjee, A.S. Kim, M. Elimelech, Concentration polarization of interacting solute particles in cross-flow membrane filtration, J. Colloid Interf. Sci. 212 (1999) 81–99.

[2] M.W. Chudacek, A.G. Fane, The dynamics of polarization in unstirred and stirred ultrafiltration, J. Membr. Sci. 21 (2) (1984) 145–160.

[3] M. Elimelech, S. Bhattacharjee, A novel approach for modeling concentration polarization in crossflow membrane filtration based on the equivalence of osmotic pressure model and filtration theory, J. Membr. Sci. 145 (1998) 223–241.

[4] C.A. Romero, R.H. Davis, Global model of crossflow microfiltration based on hydrodynamic particle diffusion, J. Membr. Sci. 39 (1988) 157–185.

[5] L.F. Song, M. Elimelech, Theory of concentration polarization crossflow filtration, J. Chem. Soc., Faraday Trans. 91 (1995) 3389–3398.

[6] J.G. Wijmans, S. Nakao, J.W.A. Van Den Berg, F.R. Troelstra, C.A. Smolders, Hydrodynamic resistance of concentration polarization boundary layers in ultrafiltration, J. Membr. Sci. 22 (1) (1985) 117–135.

[7] C.A. Romero, R.H. Davis, Experimental verification of the shear-induced hydrodynamic diffusion model of crossflow microfiltration, J. Membr. Sci. 62 (1991) 249–273.

[8] B.L. Sorensen, P.B. Sorensen, Structure compression in cake filtration, J. Environ. Eng. (1997) 345–353.

[9] A.S. Kim, E.M.V. Hoek, Cake structure in dead-end membrane filtration: Monte Carlo simulation, Environ. Eng. Sci. 19 (6) (2002) 373–386.

[10] V.V. Tarabara, I. Koyuncu, M.R. Wiesner, Effect of hydrodynamics and solution ionic strength on permeate flux in cross-flow filtration: direct experimental observation of filter cake cross-sections, J. Membr. Sci. 241 (1) (2004) 65–78.

[11] C.C. Ho, A.L. Zydney, A combined pore blockage and cake filtration model for protein fouling during microfiltration, J. Colloid Interf. Sci. 232 (2000) 389–399.

[12] B.V. Derjaguin, L.D. Landau, Theory of the stability of strongly charged lyophobic sols and of the adhesion of strongly charged particles in solutions of electrolytes, Acta Physicochim. URSS 14 (1941) 733–762.

[13] E.J. Verwey, J.T.G. Overbeek, Theory of the Stability of Lyophobic Colloids, Elsevier, Amsterdam, 1948.

[14] S. Hong, R.S. Faibish, M. Elimelech, Kinetics of permeate flux decline in crossflow membrane filtration of colloidal suspensions, J. Colloid Interf. Sci. 196 (2) (1997) 267–277.

[15] R.S. Faibish, M. Elimelech, Y. Cohen, Effect of interparticle electrostatic double layer interactions on permeate flux decline in crossflow membrane filtration of colloidal suspensions: an experimental investigation, J. Colloid Interf. Sci. 204 (1998) 77–86.

[16] J.C. Chen, A.S. Kim, Monte Carlo simulation of colloidal membrane filtration: principal issues of modeling, Adv. Colloid Interf. Sci. 119 (2006) 35–53.

[17] J.C. Chen, M. Elimelech, A.S. Kim, Monte Carlo simulation of colloidal membrane filtration: model development with application to characterization of colloid phase transition, J. Membr. Sci. 255 (2005) 291–305.

[18] H.C. Hamaker, The london–van der Waals attraction between spherical particles, Physica 4 (1937) 1058–1072.

[19] M. Elimelech, J. Gregory, X. Jia, W. Williams, Particle Deposition and Aggregation: Measurement, Modeling and Simulation, Butterworth Heinemann, Oxford, 1995.

[20] P. Meakin, Diffusion-controlled cluster formation in two, three, and four dimensions, Phys. Rev. A 27 (1) (1983) 604–607.

[21] D.A. Weitz, M. Olivera, Fractal structures formed by kinetic aggregation of aqueous gold colloids, Phys. Rev. Lett. 52 (1984) 1433–1436.

[22] D. Risovic, M. Martinis, Fractal dimensions of suspended particles in seawater, J. Colloid Interf. Sci. 182 (1) (1996) 199–203.

[23] R. Jullien, Transparency effects in cluster–cluster aggregation with linear trajectories, J. Phys. A: Math. Gen. 17 (14) (1984) L771–L776.

[24] R. Jullien, M. Kolb, Hierarchical model for chemically limited cluster–cluster aggregates, J. Phys. A: Math. Gen. 17 (1984) L639–L643.

[25] P. Meakin, Model for colloidal aggregation, Annu. Rev. Phys. Chem. 39 (1988) 237–267.

[26] P. Meakin, F. Family, Structure and dynamics of reaction-limited aggregation, Phys. Rev. A 36 (1987) 5498–5501.

[27] P. Meakin, F. Family, Structure and kinetics of reaction-limited aggregation, Phys. Rev. A 38 (1988) 2110–2123.

[28] B. Cabane, M. Meireles, P. Aimar, Cake collapse in frontal filtration of colloidal aggregates: mechanisms and consequences, Desalination 146 (1–3) (2002) 155–161.

[29] K.-J. Hwang, H.-C. Liu, Cross-flow microfiltration of aggregated submicron particles, J. Membr. Sci. 201 (1–2) (2002) 137–148.

[30] F. Pignon, A. Magnin, J.-M. Piau, B. Cabane, P. Aimar, M. Meireles, P. Lindner, Structural characterization of deposits formed during frontal filtration, J. Membr. Sci. 174 (2) (2000) 189–204.

[31] T.D. Waite, A.I. Schafer, A.G. Fane, A. Heuer, Colloidal fouling of ultrafiltration membranes: impact of aggregate structure and size, J. Colloid Interf. Sci. 212 (2) (1999) 264–274.

[32] H.C. Brinkman, A calculation of the viscous force exerted by a flowing fluid on a dense swarm of particles, Appl. Sci. Res. A1 (1947) 27–34.

[33] H.C. Brinkman, Problems of fluid flow through swarms of particles and through macromolecules in solution, Research (London) 2 (1949) 190–194.

[34] S. Veerapaneni, M.R. Wiesner, Hydrodynamics of fractal aggregates with radially varying permeability, J. Colloid Interf. Sci. 177 (1996) 45–57.

[35] M. Vanni, Creeping flow over spherical permeable aggregates, Chem. Eng. Sci. 55 (3) (2000) 685–698.

[36] A.S. Kim, R. Yuan, Hydrodynamics of an ideal aggregate with quadratically increasing permeability, J. Colloid Interf. Sci. 285 (2) (2005) 627–633.

[37] A.S. Kim, K.D. Stolzenbach, The permeability of synthetic fractal aggregates with realistic three-dimensional structure, J. Colloid Interf. Sci. 253 (2) (2002) 315–328.

[38] A.S. Kim, K.D. Stolzenbach, Aggregate formation and collision efficiency in differential settling, J. Colloid Interf. Sci. 271 (1) (2004) 110–119.

[39] P.C. Carman, Fluid flow through a granular bed, Trans. Inst. Chem. Eng. 15 (1937) 150–156.

[40] J. Happel, Viscous flow in multiparticle systems: slow motion of fluids relative to beds of spherical particles, AIChE J. 4 (1958) 197–201.

[41] J. Happel, H. Brenner, Low Reynolds Number Hydrodynamics, Kluwer, Dordrecht, 1991.

[42] K.D. Stolzenbach, Scavenging of small particles by fast-sinking porous aggregates, Deep-Sea Res. 40 (1993) 359–369.

[43] J.H. Masliyah, G. Neale, Creeping flow over a composite sphere: solid core with porous shell, Chem. Eng. Sci. 42 (2) (1987) 245–253.

[44] G. Neale, N. Epstein, W. Nader, Creeping flow relative to permeable spheres, Chem. Eng. Sci. 28 (1973) 1865–1874.

[45] A.S. Kim, R. Yuan, A new model for calculating specific resistance of aggregated colloidal cake layers in membrane filtration processes, J. Membr. Sci. 249 (2005) 89–101.

[46] R.B. Bird, W.E. Stewart, E.N. Lightford, Transport Phenomena, Wiley, New York, 1960.

[47] H. Lamb, Hydrodynamics, Dover Publications, New York, 1932.

[48] G. Ooms, P.F. Mijnlieff, H. Beckers, Friction force exerted by a flowing fluid on a permeable particle, with particular reference to polymer coils, J. Chem. Phys. 53 (1970) 4123–4130.

[49] C.N. Davies, The separation of airborne dust and particles, Proc. Inst. Mech. Eng. B1 (1952) 185–213.

[50] S. Kuwabara, The forces experienced by randomly distributed parallel circular cylinders or spheres in a viscous flow at small reynolds numbers, J. Phys. Soc. Jpn. 14 (4) (1959) 527–532.

[51] C.M. Sorensen, G.C. Roberts, The prefactor of fractal aggregates, J. Colloid Interf. Sci. 186 (2) (1997) 447–452.

[52] S.N. Rogak, R.C. Flagan, Stokes drag on self-similar clusters of spheres, J. Colloid Interf. Sci. 134 (1) (1990) 206–218.

[53] D.H. Li, J.J. Ganczarczyk, Fractal geometry of particle aggregates generated in water and wastewater treatment processes, Environ. Sci. Technol. 23 (1989) 1385–1389.

[54] A. Schmidt-Ott, New approaches to in situ characterization of ultrafine agglomerates, J. Aerosol Sci. 19 (5) (1988) 553–557.

[55] R.J. Samson, G.W. Mulholland, J.W. Gentry, Structural analysis of soot agglomerates, Langmuir 3 (2) (1987) 272–281.

[56] S.J. Jung, R. Amal, J.A. Raper, Y.M. Jo, New methodology for the analysis of physical structure of solid aggregates, J. Chem. Eng. Jpn. 35 (4) (2002) 346–353.

[57] P. Tang, J.A. Raper, Modelling the settling behaviour of fractal aggregates—a review, Powder Technol. 23 (2–3) (2002) 114–125.

[58] P. Tang, J. Greenwood, J.A. Raper, A model to describe the settling behavior of fractal aggregates, J. Colloid Interf. Sci. 247 (1) (2002) 210–219.

[59] X.-Y. Li, B.E. Logan, Permeability of fractal aggregates, Water Res. 35 (14) (2001) 3373–3380.

[60] X. Li, B.E. Logan, Collision frequencies of fractal aggregates with small particles by differential sedimentation, Environ. Sci. Technol. 31 (1997) 1229–1236.

[61] Z.-Y. Chen, P. Meakin, J.M. Deutch, Comment on "hydrodynamic behavior of fractal aggregates", Phys. Rev. Lett. 59 (18) (1987) 2121.

[62] S.P. Usher, P.J. Scales, Steady state thickener modelling from the compressive yield stress and hindered settling function, Chem. Eng. J. 111 (2–3) (2005) 253–261.

[63] S.P. Usher, P.J. Scales, L.R. White, Prediction of transient bed height in batch sedimentation at large times, AIChE J. 52 (3) (2006) 986–993.

[64] D.R. Lester, S.P. Usher, P.J. Scales, Estimation of the hindered settling function r(phi) from batch-settling tests, AIChE J. 51 (4) (2005) 1158–1168.

[65] D.N. Petsev, V.M. Starov, I.B. Ivanov, Concentrated dispersions of charged colloidal particles: sedimentation, ultrafiltration and diffusion, Colloids Surf. A: Physicochem. Eng. Aspects 81 (1993) 65.

[66] C. Kittel, Introduction to Solid State Physics, John Wiley and Sons Inc., New York, 1995.

[67] A.S. Kim, H. Chen, Diffusive tortuosity factor of solid and soft cake layers: a random walk simulation approach, J. Membr. Sci. 279 (2006) 129–139.

[68] D. Leighton, A. Acrivos, Viscous resuspension, Chem. Eng. Sci. 41 (6) (1986) 1377–1384.

[69] D. Leighton, A. Acrivos, Measurement of the shear induced coefficient of self-diffusion in concentration suspensions of spheres, J. Fluid Mech. 177 (1987) 109–131.

[70] W. Soppe, Computer simulation of random packings of hard spheres, Powder Technol. 62 (1990) 189–196.

[71] G.Y. Onoda, E.G. Liniger, Random loose packing of uniform spheres and the dilantancy onset, Phys. Rev. Lett. 64 (22) (1990) 2727–2730.

[72] G.T. Nolan, P.E. Kavanagh, Computer simulation of random packing of hard spheres, Powder Technol. 72 (1992) 149–155.

[73] P.K. Park, C.H. Lee, S. Lee, Permeability of collapsed cakes formed by deposition of fractal aggregates upon membrane filtration, Environ. Sci. Technol. 40 (8) (2006) 2699–2705.

[74] D. Nobbs, P. Tang, J.A. Raper, The design, construction and commissioning of a low-cost optical particle size analyser specifically for measurement of settling velocities and size of flocs, Meas. Sci. Technol. 13 (2002) 297–302.

[75] G.C. Bushell, Y.D. Yan, D. Woodfield, J. Raper, R. Amal, On techniques for the measurement of the mass fractal dimension of aggregates, Adv. Colloid Interf. Sci. 95 (1) (2002) 1–50.

[76] C. Lee, T.A. Kramer, Prediction of three-dimensional fractal dimensions using the two-dimensional properties of fractal aggregates, Adv. Colloid Interf. Sci. 112 (1–3) (2004) 49–57.

[77] A.D. Stickland, P.J. Scales, J.R. Styles, Comparison of geotechnical engineering consolidation and physical science filtration testing techniques for soils and suspensions, Geotech. Testing J. 28 (6) (2005) 596–604.

[78] P. Meakin, M. Muthukumar, The effects of attractive and repulsive interaction on two-dimensional reaction-limited aggregation, J. Chem. Phys. 91 (5) (1989) 3212–3221.

[79] P. Meakin, The effects of attractive and repulsive interactions on three-dimensional reaction-limited aggregation, J. Colloid Interf. Sci. 134 (1990) 235–244.

[80] G. Yang, P. Biswas, Computer simulation of the aggregation and sintering restructuring of fractal-like clusters containing limited numbers of primary particles, J. Colloid Interf. Sci. 211 (1) (1999) 142–150.